Proceedings of the 8th World Congress on New Technologies (NewTech'22)
Prague, Czech Republic– August 03-05, 2022
Paper No. ICNFA 122
DOI: 10.11159/icnfa22.122

Zno Nanowire UV Sensors by Spray-Coating and Their Transfer Length Measurement

Mindaugas Ilickas[1,2], Brigita Abakevičienė[1,2], Rasa Mardosaitė[1,2], Domantas Peckus[2], Simas Račkauskas[1,2]
[1]Department of Physics, Kaunas University of Technology
Studentų St. 50, LT-51368 Kaunas, Lithuania
mindaugas.ilickas@ktu.lt; brigita.abakeviciene@ktu.lt
[2]Institute of Materials Science of Kaunas University of Technology
K. Baršausko St. 59, LT-51423 Kaunas, Lithuania
rasa.mardosaite@ktu.lt; domantas.peckus@ktu.lt; simas.rackauskas@ktu.lt

Abstract - ZnO nanowires are commonly employed for UV sensing, however, to achieve excellent performance, a sophisticated multistep preparation procedure is necessary, as well as high measurement temperatures. In this paper, we demonstrate UV sensors manufactured by a one-step spray-coating approach based on the ZnO tetrapod (ZnO-T) structure, with high responsiveness (ON/OFF) and quick rise-decay periods at ambient temperature. The transfer length method was used to assess the ZnO-Au sensor contacts. As such UV sensors may theoretically be placed on any substrate, this technology might be employed to make UV sensors.

Keywords**:** TLM, zinc oxide, flame synthesis, coating

1. Introduction

The widespread use of zinc oxide nanostructures can be ascribed to several characteristics, the most notable of which is the material's multifunctionality [1], which allows it to be used in a wide range of applications. ZnO is one of a kind in terms of its optical, piezoelectric, magnetic, and other properties [2]. ZnO is a semiconductor with a broad bandgap (E = 3.37 eV) [3] and a relatively high nuclear binding energy (60 meV), making it a preferred choice for UV optoelectronic applications [4].

A variety of contact resistance evaluation test setups have been investigated [5]. The primary methods of contact resistance measurements are two-terminal [6], three-terminal [7], four-terminal [8], and six-terminal [9]. Many test configurations can extract the specific contact resistance [10], which can help illustrate the metal-semiconductor interface resistance. The transfer length method (TLM) provides the most comprehensive contact resistance characteristic of all the contact resistance techniques [11]. The transfer line technique allows for more than three contacts and is used as a comprehensive tool in metal-semiconductor interface characterization [9].

A flame synthesis [12] seems to have the advantage of high yield and the capacity to produce a continuous synthesis. The rates of growth of ZnO-T are extremely high. The Zn nuclei of zinc blende [13] are first generated in this way of synthesis, from which the "legs" of the wurtzite structure begin to grow [14]. Because the external temperature is higher than the melting point of zinc (419.5 °C), the zinc particles heat up and melt during the early phase. When Zn starts to evaporate, it combines with the oxygen in the air to generate saturated ZnO vapor. If Zn and O_2 are available, crystal development is closely monitored. This phase is crucial because the shape of the developing crystal is controlled by the supply of Zn and O2. Different material properties are obtained when the shape of the particle varies. A kinetic growth regime in which the rate of delivery of molecules to the surface is greater than their diffusion at the surface is required for the creation of an anisotropic shape [15], [16].

In this work we synthesized ZnO nanowires, using a spray-coating manufacture UV sensor with a rapid and high response even at room temperature and low illumination. To assess the ZnO nanowire and Au contact characteristics TLM method was used.

2. Methodology

ZnO nanotetrapods (ZnO-T) produced by fast oxidation (combustion) [15] were used to produce a UV photodetector. To dissolve the particles, 1 mg/ml solutions of isopropyl alcohol (2-propanol) were prepared and agitated in an ultrasonic bath for 10 minutes. The resulting solutions were coated on the electrodes (thickness – 200 nm (50 nm Ti and 150 nm Au), inter-electrode gap – 5 µm, 10 µm, 15 µm, width – 5 mm) at an optical thickness of 50%, which is determined by UV absorption; for example, 50% means the ZnO coating transmits 50% of UV light.

The spray nozzle had a diameter of 0.5 mm, and compressed air was used as the transporting gas (1.5 MPa). The distance between the platform and the nozzle was around 10 cm. The current-voltage (I–V) parameters were measured using a Keithley 6487 picoammeter. A 365 nm UV light source was used to measure the optical thickness of ZnO-T. The optical properties of the ZnO coatings were studied using AvaSpec-2048 UV-VIS-NIR (Light source - deuterium and halogen. Spectral range 172-1100 nm, resolution 1.4 nm) in the range 200-800 nm wavelength. Transmission electron microscopy (TEM) images were taken by Tecnai G2 F20 X-TWIN (FEI) with a Schottky-type field emission electron source. The structural characteristics of ZnO powder were investigated using a D8 Discover X-ray diffractometer (Bruker AXS GmbH) equipped with a Cu K (λ = 1.5418 Å) radiation source and a 60 mm Göbel mirror in a parallel beam geometry.

3. Results

The ZnO-T structure is made up of four legs that are joined at one end and spread uniformly in all directions, as seen in Figure 1 from TEM images. The leg diameter and length are 30 – 40 nm and 0.3 – 0.5 µm, respectively, resulting in a 10-15 aspect ratio. The inset of Figure 1 shows a tip of the ZnO-T leg, illustrating the ZnO-T structure's exceptional crystallinity.

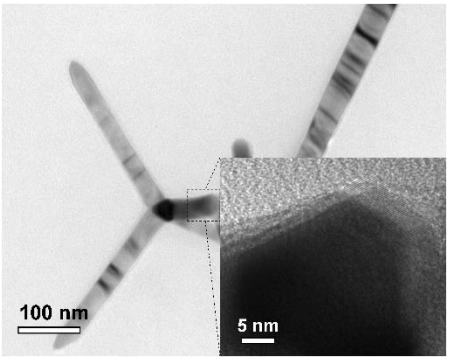

Fig. 1: TEM investigation of ZnO nanotetrapods (ZnO-T). Inset shows a closeup of one ZnO-T leg.

Figure 2 shows ultraviolet-visible spectroscopy (UV-Vis) of ZnO-T nanoparticles. Synthesized particles (ZnO-T) show a characteristic intensity peak at the 370-380 nm wavelength region.

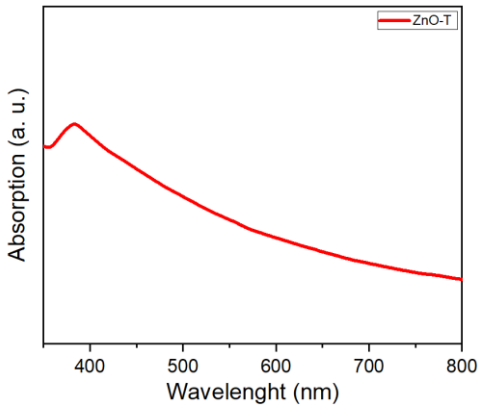

Fig. 2: UV-Vis's absorption spectra of ZnO-T nanoparticles.

Figure 3 shows a typical particle X-ray diffraction (XRD) pattern of generated ZnO-T structures. All XRD peaks were were identified by hexagonal wurtzite crystal structure [17] of ZnO with the most preferred orientations (100), (002), and and (101), in accordance with the JCPDS database (card. No. 00 036-1451). The intense and narrow diffraction peaks of of ZnO reveal its nanocrystalline structure [18].

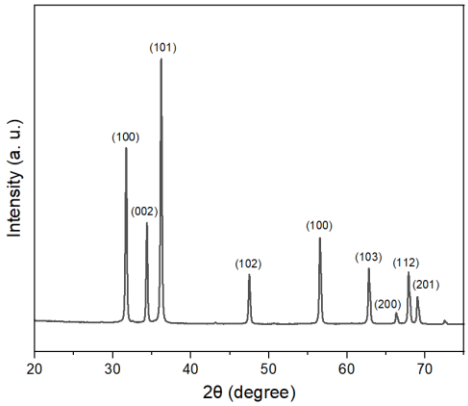

Fig. 3: XRD spectra of ZnO-T nanoparticles.

The UV detecting properties of spray-coated UV photodetectors are shown in Figure 4. Figure 4(a) shows the typical I–V characteristics of the UV detector with and without 0.31 mW/cm^2 UV light. The linear increase suggested the creation of Ohmic contacts between Au and ZnO nanowires. The currents were 54.6 × 10^{-5} μA, 9.12 × 10^{-5} μA, and 4.04 × 10^{-5} μA at -5 V for inter-electrode intervals of 5 μm, 10 μm, and 15 μm, respectively, without UV irradiation. Otherwise, at -5 V, the current surged to 48.1 × 10^{-2} μA, 2.51 × 10^{-2} μA, and 3.05 × 10^{-2} μA for inter-electrode intervals of 5 μm, 10 μm, and 15 μm, respectively, under UV light of 0.31 mW/cm^2. Furthermore, at inter-electrode distances of 5 μm, 10 μm, and 15 μm, the photocurrent to the dark current ratio (ON-OFF current ratio) was 880, 275, and 755, respectively.

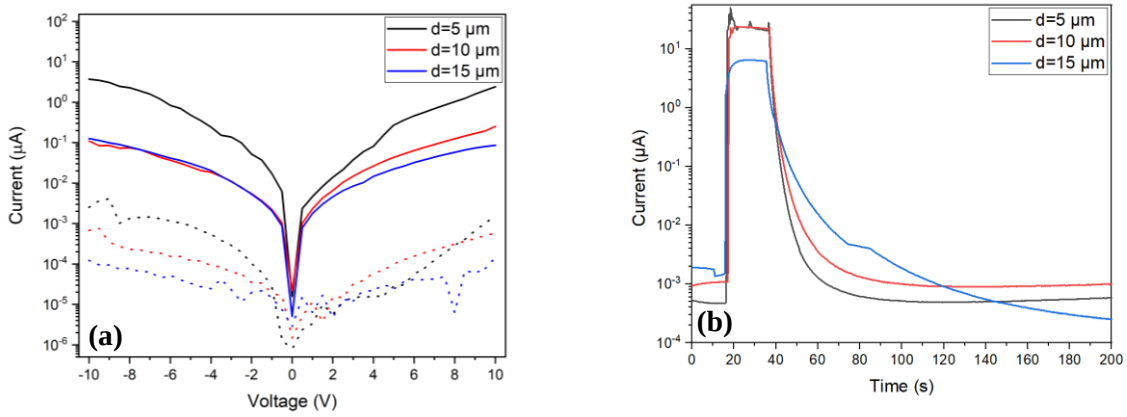

Fig. 4: (a) Current-voltage characteristics of ZnO-T particles, dot line present dark mode and solid line measurements at UV light; (b) Current-time response curves.

The current-time response curves of our produced device are shown in Figure 4(b). The sensor with the fastest rising time has a 5 μm inter-electrode gap – 0.52 s. Sensors with larger spacing were slower: 10 μm inter-electrode gap – 0.81 s, and 15 μm inter-electrode gap – 2.32 s, respectively. Sensors with inter-electrode gaps of 5 μm – 15.44 s had the fastest

decay time, whereas sensors with inter-electrode gaps of 10 μm – 18.46 s and sensors with inter-electrode gaps of 15 μm – 64.55 s had the slowest decay time. The longer percolation path across electrodes, which also contains more inter-leg connections, could explain the wider gap relationship to slower reaction. This lowers current flow due to the increased number of barriers, which affects overall performance.

Figure 5 shows the dependence of the resistance on the gap between the electrodes and on the use of UV light. The blue part of the graph means that the UV has been turned off and the red part means that the UV light has been turned on. Looking at the part where there was no UV light, values changed 2 orders of magnitude, and when the UV light was on, only 1 order of magnitude changed.

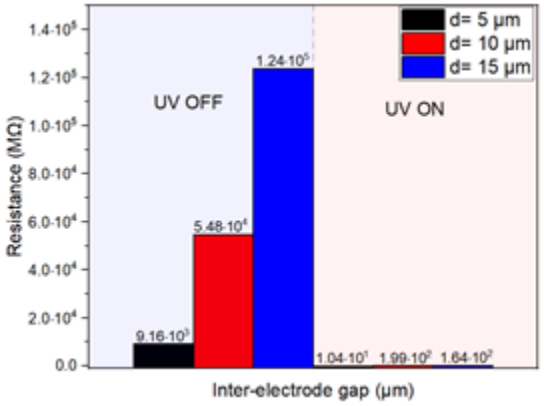

Fig. 5: Resistance dependence on the inter-electrode gap.

The total resistance values (see Figure 5) are high, which leads to a large transfer length (0.95 mm and 2.27 mm). The contact, sheet, and specific contact resistances for the sensor without UV light are calculated as 26036.65 MΩ, 57341.90 MΩ/□, and 2955.54 MΩ/cm^2. The same parameters for a sensor with UV light illumination are 14.54 MΩ, 46.09 MΩ/□, and 0.41 MΩ/cm^2 respectively.

The total resistance R_T across two contacts with length (Z) and width (L) is calculated and plotted versus contact spacing d when using the TLM technique (shown in Figure 1). From this graph, three variables can be extracted: contact resistance (R_C), sheet resistance (R_{sh}), and transfer length (L_T). The effect of sheet resistance on total resistance measurement increases as contact spacing d increases, leading to the slope of the TLM plot (k) [19].

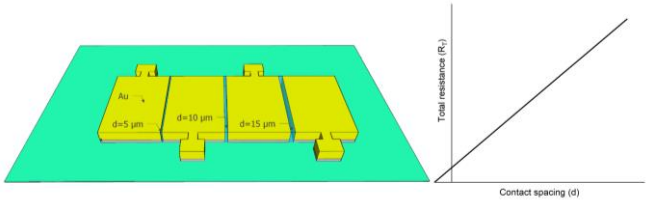

Fig. 6: (a) sensor schematic view. (b) The fitted curve of total resistance (R_T) versus contact spacing (d).

The value of sheet resistance (R_{sh}) can be calculated using [19]:

$$\frac{\Delta R_T}{\Delta d} = \frac{R_{sh}}{z} = k \tag{1}$$

The mean difference along with L over which current moves from the semiconductor to the metal and vice versa is referred to as the transfer length. It is defined as follows [19]:

$$L_T = \sqrt{\frac{\rho_c}{R_{sh}}} \tag{2}$$

The total resistance at the plot's y-intercept is $2R_C$. R_C can be found using the potential distribution beneath the contact, which is represented by:

$$R_c = \frac{\rho_c}{L_T Z} \tag{3}$$

The total resistance between any two contacts can be expressed as [20]:

$$R_T = \frac{R_{sh} d}{Z} + 2R_c \approx \frac{R_{sh}}{Z}(2 + L_T) \tag{4}$$

Table 1: Main parameters from TLM measurements.

UV	ON	OFF
R_C, MΩ	14.54	26036.65
R_{Sh}, MΩ/□	46.09	57341.90
L_T, mm	0.95	2.27
ρ_C, MΩ·cm^2	0.41	2955.54

Table 1 shows the main TLM measurement parameters for measurements made without UV illumination (OFF) and with UV illumination (ON). It can be noticed that in both measurement cases L_T is in the range of millimeters (0.95-2.27 mm), meaning that for effective sensor performance contacts should be at least 2.27 mm wide or more.

4. Conclusion

In summary, a spray-coating technique was used to create a UV photodetector. The dynamic sensing response of the spray-coated devices was steady and repeatable. Under UV irradiation of 0.31 mW/cm^2 and an applied voltage bias of -5 V, the devices demonstrated an ON/OFF current ratio of 275-880 and a recovery period of 15.44-64.55 s. A decreasing trend in the contact resistivity is observed with the usage of UV light illumination. For an effective ZnO nanowire sensor performance, contact width should not be less than 2.27 mm, which is important in nanowire sensor manufacture.

Acknowledgments

This research is funded by the European Regional Development Fund according to the supported activity "Multifunctional coatings based on ZnO nanowires for selective sensing and efficient solar harvesting (MultiFun)", project No. 01.2.2-LMT-K-718-02-0011.

References

[1] J. Jiang, J. Pi, and J. Cai, "The Advancing of Zinc Oxide Nanoparticles for Biomedical Applications," *Bioinorganic Chemistry and Applications*, vol. 2018, p. 1062562, 2018, doi: 10.1155/2018/1062562.

[2] Y. K. Mishra and R. Adelung, "ZnO tetrapod materials for functional applications," *Materials Today*, vol. 21, no. 6, pp. 631–651, 2018, doi: https://doi.org/10.1016/j.mattod.2017.11.003.

[3] V. A. Coleman and C. Jagadish, "Chapter 1 - Basic Properties and Applications of ZnO," in *Zinc Oxide Bulk, Thin Films and Nanostructures*, C. Jagadish, and S. Pearton, Eds. Oxford: Elsevier Science Ltd, 2006, pp. 1–20. doi: https://doi.org/10.1016/B978-008044722-3/50001-4.

[4] S. Rackauskas, K. Mustonen, T. Järvinen, M. Mattila, O. Klimova, H. Jiang, O. Tolochko, H. Lipsanen, E. Kauppinen, and A. Nasibulin, "Synthesis of ZnO tetrapods for flexible and transparent UV sensors," *Nanotechnology*, vol. 23, no. 9, p. 095502, 2012, doi: 10.1088/0957-4484/23/9/095502.
[5] K. Kamimura, S. Okada, M. Nakao, Y. Onuma, and S. Yamashita, "Characterization of contact resistance of low-value resistor by transmission line model (TLM) method," *Electronics and Communications in Japan (Part II: Electronics)*, vol. 85, no. 3, pp. 16–22, Mar. 2002, doi: https://doi.org/10.1002/ecjb.1095.
[6] R. H. Cox and H. Strack, "Ohmic contacts for GaAs devices," *Solid-State Electronics*, vol. 10, no. 12, pp. 1213–1218, 1967, doi: https://doi.org/10.1016/0038-1101(67)90063-9.
[7] H. Murrmann and D. Widmann, "Current crowding on metal contacts to planar devices," *IEEE Transactions on Electron Devices*, vol. 16, no. 12, pp. 1022–1024, 1969, doi: 10.1109/T-ED.1969.16904.
[8] S. J. Proctor, L. W. Linholm, and J. A. Mazer, "Direct measurements of interfacial contact resistance, end contact resistance, and interfacial contact layer uniformity," *IEEE Transactions on Electron Devices*, vol. 30, pp. 1535–1542, 1983.
[9] Dieter K. Schroder, *Semiconductor Material and Device Characterization*, 3rd ed. Wiley-IEEE Press, 1990.
[10] S. E. Mohney, Y. Wang, M. A. Cabassi, K. K. Lew, S. Dey, J. M. Redwing and T. S. Mayer, "Measuring the specific contact resistance of contacts to semiconductor nanowires," *Solid-State Electronics*, vol. 49, no. 2, pp. 227–232, 2005, doi: https://doi.org/10.1016/j.sse.2004.08.006.
[11] W. Shockley, A. Goetabarger, and R.M. Scarlett, "Research and Investigation of Inverse Mitaxial UHF Power Transistors," 1964
[12] D. Gedamu, I. Paulowicz, S. Kaps, O. Lupan, S. Wille, G. Haidarschin, Y. K. Mishra and R. Adelung, "Rapid Fabrication Technique for Interpenetrated ZnO Nanotetrapod Networks for Fast UV Sensors," *Advanced Materials*, vol. 26, no. 10, pp. 1541–1550, Mar. 2014, doi: https://doi.org/10.1002/adma.201304363.
[13] Y. Ding, Z. L. Wang, T. Sun, and J. Qiu, "Zinc-blende ZnO and its role in nucleating wurtzite tetrapods and twinned nanowires," *Applied Physics Letters*, vol. 90, no. 15, p. 153510, Apr. 2007, doi: 10.1063/1.2722671.
[14] A. Ashrafi and C. Jagadish, "Review of zincblende ZnO: Stability of metastable ZnO phases," *Journal of Applied Physics*, vol. 102, no. 7, p. 071101, Oct. 2007, doi: 10.1063/1.2787957.
[15] S. Rackauskas, O. Klimova, H. Jiang, A. Nikitenko, K. A. Chernenko, S. D. Shandakov, E. I. Kauppinen, O. V. Tolochko, and A. G. Nasibulin, "A Novel Method for Continuous Synthesis of ZnO Tetrapods," *The Journal of Physical Chemistry C*, vol. 119, no. 28, pp. 16366–16373, Jul. 2015, doi: 10.1021/acs.jpcc.5b03702.
[16] Rackauskas S., Ed., *Flexible Electronics*. London, United Kingdom: IntechOpen, 2018. ISBN978-1-78923-457-2.
[17] J. Singh Galsin, *Solid State Physics An Introduction to Theory*. Academic Press, 2019.
[18] N. Xu, Y. Cui, Z. Hu, W. Yu, J. Sun, N. Xu, and J. Wu, "Photoluminescence and low-threshold lasing of ZnO nanorod arrays," *Optics Express*, vol. 20, no. 14, pp. 14857–14863, 2012, doi: 10.1364/OE.20.014857.
[19] S. Guo, G. Gregory, A. M. Gabor, W. v Schoenfeld, and K. O. Davis, "Detailed investigation of TLM contact resistance measurements on crystalline silicon solar cells," *Solar Energy*, vol. 151, pp. 163–172, 2017, doi: https://doi.org/10.1016/j.solener.2017.05.015.
[20] F. Shereen, "Transfer Length Measurements For Different Metallization Options And Processing Of Gallium Tin Zinc Oxide (Gszo) Tfts," 2011.